Atomic layer deposited ZnO:B as transparent conductive oxide for silicon heterojunction solar cells

Available online at www.sciencedirect.com

ScienceDirect

Energy Procedia 92 (2016) 624 – 632

Energy Procedia

6th International Conference on Silicon Photovoltaics, SiliconPV 2016

Atomic layer deposited ZnO:B as transparent conductive oxide for increased short circuit current density in silicon heterojunction solar cells

Henriette A. Gatz[a,*], Dibyashree Koushik[a], Jatin K. Rath[b], Wilhelmus M. M. Kessels[a,c], Ruud E. I. Schropp[a,c]

[a]*Eindhoven University of Technology, Department of Applied Physics, Postbus 513, 5600 MB Eindhoven, The Netherlands*
[b]*Utrecht University, Faculty of Science, Debye Institute for Nanomaterials Science - Physics of Devices, High Tech Campus 21, 5656 AE Eindhoven, The Netherlands*
[c]*Solliance, High Tech Campus 21, 5656 AE Eindhoven, The Netherlands*

Abstract

A key factor to improve the performance of silicon heterojunction solar cells (SHJ) is increasing their short circuit density (J_{sc}) by reducing the parasitic absorption of light in the front side of the cell. Therefore, we have investigated the replacement of the conventional sputtered ITO on the SHJ front side with highly transparent boron doped zinc oxide (ZnO:B). The ZnO:B is prepared by atomic layer deposition (ALD) with the novel triisopropyl borate precursor, $B(O^iPr)_3$ (TIB), which presents an easy controllable and safer alternative to commonly used boron precursors.

Outstanding J_{sc} values of 35.50 mA/cm^2 for cells on double sided polished wafer (DSP) and 38.76 mA/cm^2 for cells on textured wafer are observed for SHJ cells with ZnO:B, as compared to 33.48 mA/cm^2 (DSP) and 37.31 mA/cm^2 (textured) for reference cells with ITO. The potential of ZnO:B grown with TIB as indium-free TCO with increased transmission for SHJ solar cells is thereby demonstrated. Furthermore, indium free SHJ solar cells with ALD deposited ZnO:B as front TCO and ZnO:Al as back TCO have been successfully demonstrated.

Peer review by the scientific conference committee of SiliconPV 2016 under responsibility of PSE AG.

Keywords: ZnO:B; triisopropyl borate, TIB; ALD; SHJ solar cells;

Peer review by the scientific conference committee of SiliconPV 2016 under responsibility of PSE AG.
doi:10.1016/j.egypro.2016.07.028

1. Introduction

Silicon Heterojunction (SHJ) solar cells are well known for holding the record efficiency of 25.6% in back contacted configuration for crystalline silicon based solar cells [1]. An important difference with previous world records lies in the fully back contacted configuration of the cells, which shows that light in-coupling is one of the key factors for good SHJ solar cell performance. For conventional contacted SHJ solar cells, a high performance of the front TCO is required. It needs to be reasonably low resistive (< 10^{-3} Ωcm), while still maintaining high transmission (> 80%) in order to allow a large amount of light to reach the active absorber layer of the cell and thus generate a high short circuit current density J_{SC}. The most commonly used transparent conductive oxide (TCO) for SHJ solar cells in production is indium-doped tin oxide (ITO). However, an indium free alternative is desirable due to the scarcity of this element.

A commonly used precursor for boron doping in atomic layer deposition (ALD) processes is diborane, which is extremely flammable, very toxic, fatal if inhaled, and causes severe skin burns and serious eye damage [2]. Triisopropyl borate (TIB) in comparison is so far only known to be highly flammable, expected to be a low ingestion hazard, might be harmful after prolonged inhalation, and might cause temporary eye and skin irritations. Regarding toxicity of TIB, till now only limited data are available [3,4], but TIB potentially is a much safer alternative. Moreover, TIB has a favorable lower vapor pressure of 13 Torr at 25°C, compared to diborane with 3.5×10^4 Torr at 25°C [5].

ALD prepared boron doped zinc oxide (ZnO:B) with the TIB precursor as a boron-source has recently been developed by Garcia-Alonso et al. [5]. We present to our knowledge the first implementations of this new type TCO in SHJ solar cells. In this paper, the performance of SHJ solar cells with conventionally sputtered ITO and the novel ZnO:B layer is compared, showing a clear increase of J_{SC} for cells with ZnO:B. In addition, indium free SHJ solar cells are realized using ZnO:B as front TCO and aluminum doped zinc oxide (ZnO:Al) as rear TCO.

2. Experiment

All ZnO layers are deposited via ALD in an OpAL™ reactor from Oxford Instruments. Diethyl zinc ($(C_2H_5)_2Zn$, DEZ > 99.999%, Dockweiler Chemicals)) and triisopropyl borate ($B(O^iPr)_3$, TIB > 98%, Air Liquide) or trimethylaluminium ($Al_2(CH_3)_6$, TMA > 99.99%, Dockweiler Chemicals) served as precursor gasses. For material characterization, 75 nm thick ZnO:B layers (the thickness commonly used in SHJ cells) have been grown on silicon wafers covered with a thermally grown SiO_2 layer as well as on 7059 Corning glass. The sheet resistance R_{sh} has been determined by four point probe measurements, the optical transmission T_{opt} was studied using a UV-VIS-NIR spectrometer (Carry 5000, Agilent technologies). The transmission data are corrected for reflection by comparing to a bare Corning glass substrate.

The optical properties of the ALD ZnO:B for different doping fractions were investigated using a J.A. Woollam, Inc. M2000 UV ellipsometer. The data were analyzed using a Psemi-M0 model [6] to extract the refractive index (n), extinction coefficient (k), and the absorption coefficient (α). The optical bandgap E_g was determined by linear extrapolation of the so called Tauc plots, which present $(\alpha h\nu)^2$ vs $h\nu$.

SHJ solar cells have been fabricated on textured <100> n-type Cz wafers (thickness ~150 µm), and on double side polished (DSP) <111> n-type FZ c-Si wafers (thickness ~ 275 µm). Figure 1 shows an overview of the different samples. The arrangement of all thin-film silicon layers is the same for each sample, whereas the TCO material (and for sample type IV also the front contact material) varies. In cell type I the ALD prepared ZnO:B is implemented as front TCO with ITO as back TCO. Cell type II serves as reference with ITO as front and back TCO. Both cell types are made on DSP as well as on textured wafer.

Cell type III realizes an indium free SHJ solar cell by using ZnO:B as front TCO and ZnO:Al as back TCO on a DSP wafer. Cell type IV (on textured wafer), with ZnO:B as front TCO, ITO as back TCO, and gold (Au) as front grid contact is used for annealing studies.

All wafers are coated with a 5-nm intrinsic amorphous silicon layer (a-Si:H(i)) in the PASTA reactor [7] on both sides. The rear is then coated with 20 nm a-Si:H(n), 75 nm TCO (ITO, or in case of cell type III ZnO:Al), and 200 nm silver (Ag). The front side emitter layer consist of 5 nm nc-Si:H(p) to facilitate a fast nucleation of the silicon oxide layer, a 12 nm nc-SiO_x:H(p) highly transparent emitter layer, and a 3 nm nc-Si:H(p) layer to improve

the contact to the top TCO [8]. The passivating intrinsic layers are deposited by hot wire chemical vapor deposition (HWCVD), the doped layers are deposited via plasma enhanced chemical vapor deposition (PECVD).

As front TCO 75 nm of either rf-magneton sputtered ITO (sample type II) or ALD prepared ZnO:B (all other sample types) is used. During the ITO deposition, the solar cell area of 1 cm × 1 cm is defined by a mask.

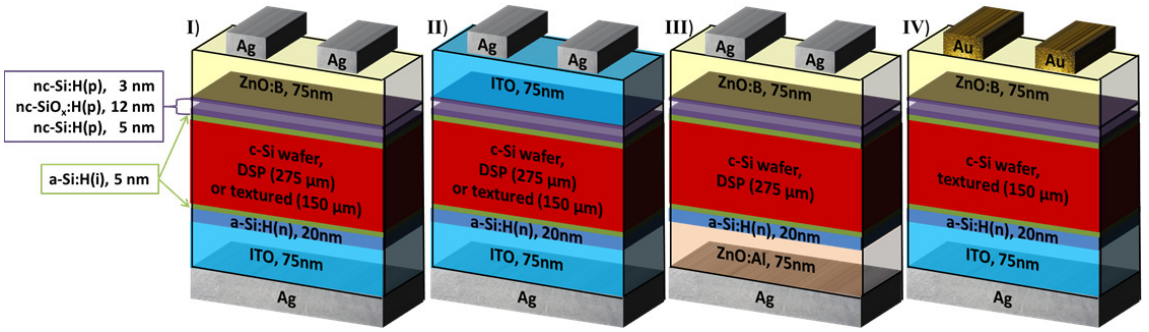

Fig. 1. Schematic overview of the different investigated silicon heterojunction (SHJ) solar cells studied in this work. In purple on the SHJ solar cell front side, the 5-nm nc-Si:H(p) nucleation promoting layer, the 12 nm highly transparent nc-SiO_x:H(p) emitter layer, and the 3 nm nc-Si:H(p) contact layer are indicated. Solar cell type I and II are realized on double sided polished (DSP) as well as on textured wafer. Cell type III is made on DSP wafer and cell type IV on textured wafer.

ZnO:B and ZnO:Al are prepared by ALD. Doping is achieved by performing *m* cycles of ZnO ALD, each cycle consisting of a sequence of DEZ dosing, purging, water vapor dosing, and purging, followed by one cycle of the dopant material. To achieve the desired film thickness this supercycle (*m*+1) is repeated as needed. Figure 2 shows a schematic overview of the ZnO:B ALD deposition scheme. The dopant cycle ratio *R* is determined as $R = 1/(m+1)$. ZnO:Al is deposited with a dopant cycle ratio of $R = 0.042$ on the rear of cell type III.

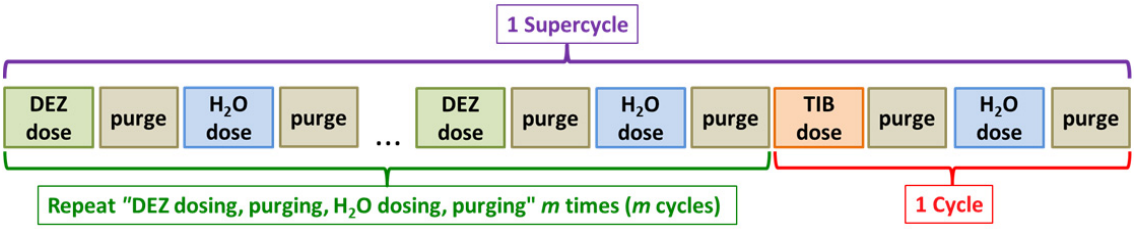

Fig. 2. Overview of the deposition steps of the ALD process of ZnO:B, indicating the variable number of ZnO deposition cycles *m* after which one dopant cycle is introduced, together forming a complete supercycle.

Due to the nature of the ALD process, the ZnO:B is deposited on the complete solar cell front side of sample type I, III, and IV. Their individual cells are subsequently separated by cleaving the wafer. On top of the TCO, evaporated silver or gold grids serve as front contacts.

To guarantee good interface passivation, as well as a good contact between the TCO and the metallization, the finished solar cells of sample type I-III are annealed for 3h at 180°C under nitrogen atmosphere.

Sample type IV is dedicated to annealing studies. The samples are therefore after deposition of the front and back TCO pre-annealed for 30 min at 170°C in vacuum prior to the Au deposition. After the Au evaporation, the cells are annealed in consecutive steps between 130 - 240°C. The illuminated current density - voltage (*J-V*) characteristics are determined after each annealing step.

The *J-V* characteristics of all cell types are determined with a WACOM dual beam solar simulator under AM1.5 illumination, using a shadow mask to accurately define the cell area of 1 cm^2. Due to human limitations in accuracy of placing the mask, the data are corrected by rescaling for the J_{SC} retrieved from *EQE* measurements.

The series resistance R_S and the parallel resistances R_P are determined under illumination conditions. They are calculated as the inverse of the slope near open circuit and short circuit conditions respectively. The External Quantum Efficiency (*EQE*) is determined with an Optosolar (SR300) setup equipped with a 250 W xenon lamp and a Jobin Yvon iHR320 monochromator.

3. Results and discussion

We investigated the relevant material properties of ALD ZnO:B for 75-nm thick layers, which is the optimum TCO thickness for SHJ solar cells. The doping fraction $DF = \frac{at\%_B}{at\%_B + at\%_{Zn}}$ with $at\%_B$ being the atomic percentage of boron and $at\%_{Zn}$ being the atomic percentage of zinc in the material, has been investigated by Garcia-Alonso et al. [5] for ZnO:B prepared by ALD at 150°C. It has been found, that the *DF* is a linear function of the dopant cycle ratio *R*, with a higher dopant cycle ratio leading to a higher doping fraction and thus higher incorporation of boron in the film.

Figure 3a) shows the sheet resistance R_{sh} of these layers grown on Corning glass as well as on thermal oxide coated wafer. The sheet resistance exhibits a favourable minimum at $R = 0.040$ ($m = 24$). This behaviour can be explained by the doping efficiency of the material. The doping efficiency is the ratio between doping induced excess carrier density and dopant density:

$$\eta_{doping} = \frac{n-n_0}{N_{Zn} \cdot D_F} \cdot 100\%,$$

with n being the carrier density of an intrinsic ZnO film, n_0 the carrier density of a doped film, N_{Zn} the atomic density of Zn and *DF* the doping fraction [5]. Garcia Alsonso et al. found, that for small doping fractions, η_{doping} rises with increasing doping fraction. After reaching a peak value η_{doping} decreases with further increase of the doping fraction. As can be seen, the sheet resistance decreases with increasing deposition temperature. This is attributed to an increase in mobility as well as an increase in carrier concentration of the material with increasing deposition temperature [5].

Due to the favorable decrease of sheet resistance with increasing deposition temperature, a temperature of 200°C, which is commonly the highest temperature suitable for SHJ solar cell production, has been chosen for all following experiments. In order to evaluate the suitability of ZnO:B as a front TCO for SHJ solar cells, its optical properties have been investigated. As shown in Figure 3b), all layers exhibit good transmission over a large wavelength range, which makes them optically favorable over ITO as front TCO.

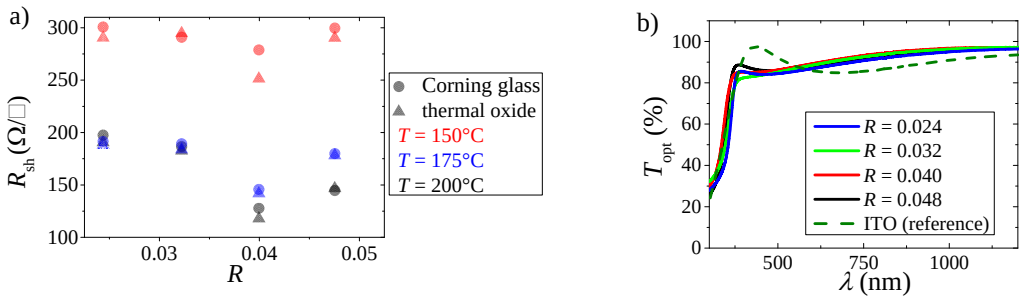

Fig. 3. a) Sheet resistance R_{sh} for different dopant cycle ratios *R* deposited on Corning glass (circles) and thermal oxide (triangles) for different deposition temperatures *T*. For reference: R_{sh} (ITO) = 48 Ω/□ on Corning glass. b) Transmission T_{opt} (for $T = 200$°C) for 75 nm thin films as a function of the wavelength λ for different dopant cycle ratios.

Since the transmittance of the thin films on glass is influenced by its thickness (here 75 nm for all films) as well as by interference effects in the film, the optical properties have further been investigated. Figure 4 a) and b) show the refractive index *n* and the extinction coefficient *k*, for ALD ZnO:B films deposited with various dopant cycle ratios *R* at 200°C. As can be seen in Figure 4a, at a given wavelength λ the refractive index *n* decreases with

increasing dopant cycle ratio R and thus increasing boron content in the films. The same behaviour can be observed in Figure 4b) for the extinction coefficient k. At a given λ, k decreases with increasing R (in the low wavelength range). These behaviours of n and k are known and have been attributed to an increase in the carrier concentrations in the material [9], which has been found for increasing doping fraction in the doping ratio range we investigated [5]. This is related to a change in bandgap, that we will discuss below.

Figure 4c shows the absorption coefficient α as a function of the photon energy E_{ph}. A blue shift is clearly visible in the absorption edge of the ZnO:B with increasing boron doping ratio R. The incorporation of boron in the material provides free charge carriers that shift the Fermi level into the conduction band and thus widen the band gap according to the Burstein–Moss theory [5,9]. The Tauc plot ($(\alpha h\nu)^2$ vs. $h\nu$) of the different ZnO:B films is shown in Figure 4 d). As can be seen in the inset of the figure, the optical band gap E_g increases with increasing R, and thus with increasing boron incorporation, which is in agreement with the previous reported studies on ZnO:B deposited by ALD or sol-gel method [5,9-11]. The Burstein-Moss shift could be the dominant reason for this band gap widening. Moreover, additional effects such as strain, grain size, and imperfections in the lattice might contribute to this widening as well [11].

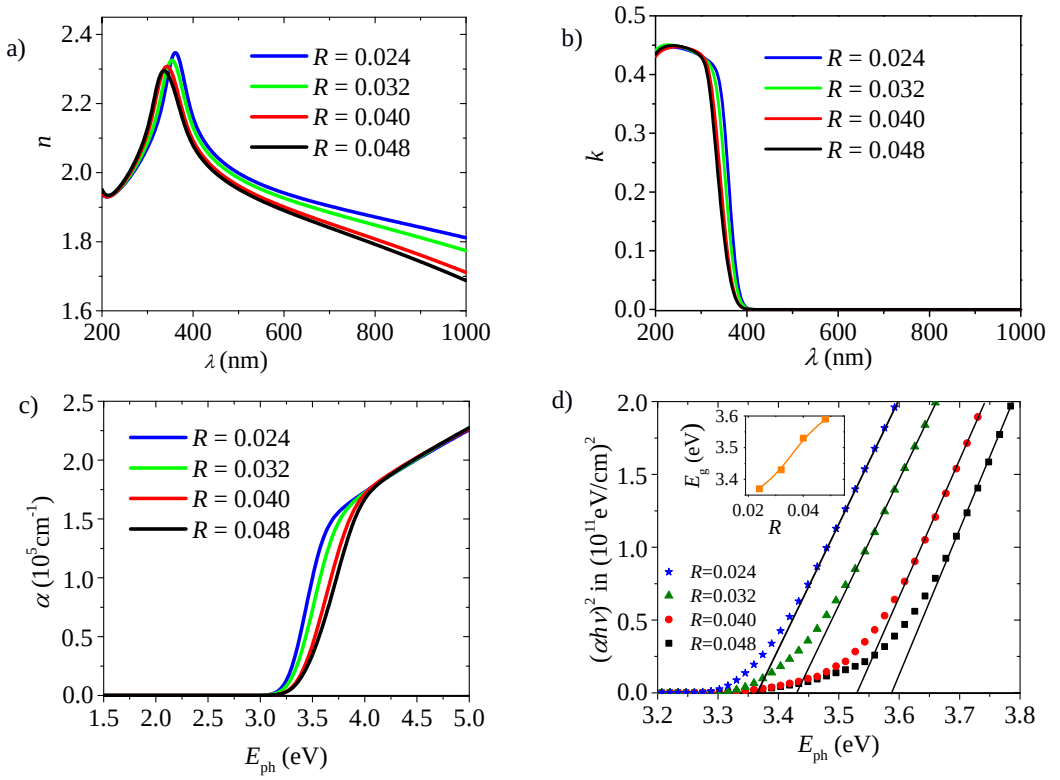

Fig. 4. Optical parameters of the ZnO deposited with different doping ratios R at 200 °C: a) Refractive index n and b) extinction coefficient k as a function of the wavelength λ. c) Absorption coefficient α and d) Tauc plot with $(\alpha h\nu)^2$ as a function of photon energy E_{ph}. Inserted frame: optical band gap E_g for the different doping ratios.

All investigated ZnO:B materials show good optical properties for all doping ratios. Therefore, the most conductive ZnO:B, grown with R = 0.040 (T = 200°C), has been chosen for implementation in the SHJ solar cells. The resistivity of the selected ZnO:B layer is 9.1×10^{-4} Ω·cm on Corning glass, whereas the resistivity for our standard sputtered ITO is 3.6×10^{-4} Ω·cm for 75 nm thick layer.

Figure 5 shows the illuminated *J-V* characteristics of the SHJ solar cells. As can be seen, the cell with ZnO:B exhibit an impressive gain in J_{SC} of almost 4% for cells on textured wafers (Figure 5a) and more than 6% for cells on double side polished (DSP) wafers (Figure 5b) compared to cells with ITO. This results in outstanding values of J_{SC} = 35.50 mA/cm^2 (DSP) and 38.76 mA/cm^2 (textured). We attribute this to the higher transparency of the ZnO:B. Figure 5c further illustrates the benefits of ZnO:B over ITO observed by external quantum efficiency (*EQE*) measurements for all cell types.

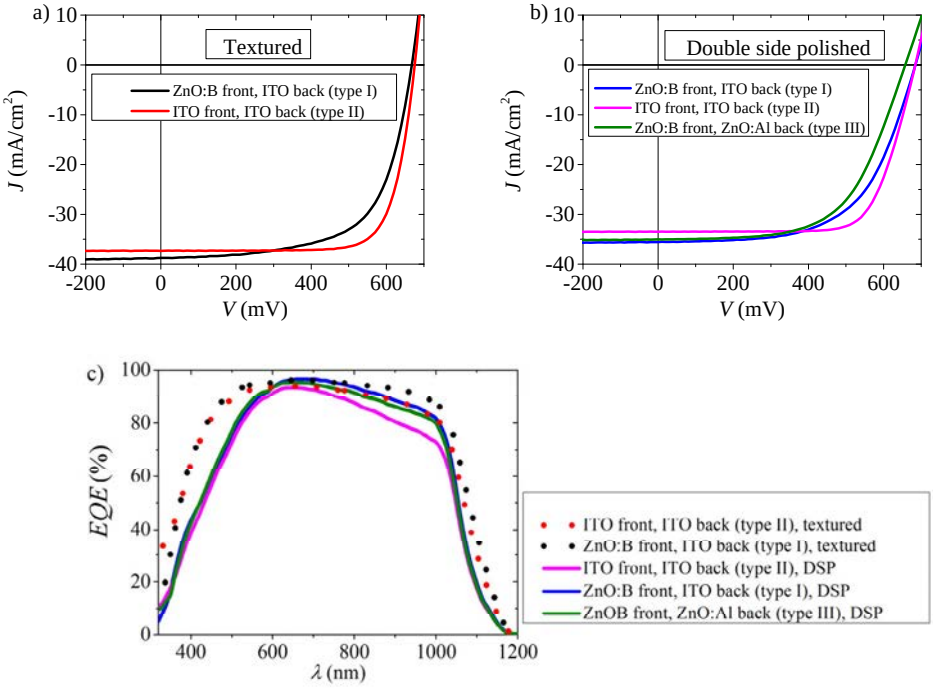

Fig. 5. Comparison of *J-V*-curves for SHJ solar cells of sample type I and II on textured wafer (a) and sample type I-III on double side polished (DSP) wafer (b). c) Wavelength dependent *EQE* (measured at short circuit condition without bias light) for the same solar cells.

Table 1 shows an overview of the solar cell parameters of the different types of solar cells. Unfortunately, the cells including ZnO:B suffer from a less favourable fill factor (*FF*), and thus lower efficiency (η). This can be attributed to the higher resistivity of ZnO:B, leading to a higher series resistance (R_S). Furthermore, the cells with ZnO:B have an unfavourable lower parallel resistance (R_P). Additional factors such as the work function might also have an influence that we will be discussed later in detail.

Not much difference in *FF*, J_{sc}, and η is visible for cells with ZnO:B front and ZnO:Al back TCO (sample type I) compared to ZnO:B front and ITO back TCO (sample type III). The decrease in V_{OC} for cells with ZnO:Al could be attributed to a lower work function of the ZnO:Al compared to ITO, possibly resulting in a reduced field effect passivation [12]. However, we strongly suspect difficulties during the cleaving of the type III cell might have resulted in edge defects and thus contributed to or entirely caused the lower V_{OC} of these cells.

An additional factor, other than the series and parallel resistance, seems to influence the *FF*. This might be related to the work function of the ZnO:B. It can be seen in the work of Varache et al. [13] as well as Bivour et al. [14], that it is possible to observe a decrease of *FF* at smaller changes in work function and much more pronounced compared to the decrease of V_{OC}.

Table 1. SHJ solar cell parameters.

Sample type*	Wafer type	Front TCO	Back TCO	V_{OC} (mV)	J_{SC} (mA/cm^2)	*FF* (%)	η (%)	R_S (Ω·cm^2)	R_P (Ω·cm^2)
I	DSP	ZnO:B	ITO	0.685	35.50	0.60	14.53	3.9×E+0	1.3×E+3
II	DSP	ITO	ITO	0.684	33.48	0.72	16.53	3.1×E+0	1.2×E+4
III	DSP	ZnO:B	ZnO:Al	0.658	35.05	0.66	13.81	4.4×E+0	1.2×E+3
I	textured	ZnO:B	ITO	0.668	38.76	0.64	16.68	1.9×E+0	6.1×E+2
II	textured	ITO	ITO	0.675	37.31	0.76	19.23	1.3×E+0	1.1×E+4

* Please refer to Figure 1 for the sample type numbers.

The work function is not considered a material constant, since it can largely vary depending on the material preparation. Factors like the surface dipole (which can increase the work function due to an increase in ion potential) and carrier doping (which lowers the work function) influence its value. However, extensive studies on layers grown by DC magneton sputtering, RF magneton sputtering, and ceramic sintering have observed a general trend of remarkable lower work functions for ZnO and ZnO:Al compared to ITO. We expect the same for ZnO:B. A range of typical work functions of 3.1 eV - 4.5 eV for ZnO:Al and 3.6 eV - 5.3 eV for ITO has been found [15]. Hence, it is realistic to assume that the ZnO:B we implemented has a lower work function than the ITO.

Rößler et al. found for SHJ with conventional a-Si:H(p) emitter layer, that a too low TCO work function will result in a decrease in *FF*. A high work function, leading to a small work function difference between the emitter and the TCO layer, is necessary in order to achieve flat band conditions. Otherwise, depletion at the emitter layer is introduced [12]. This is supported by Chen et al., who predicted a high efficiency SHJ solar cell only for large work functions [16].

In order to have a good contact between the TCO and the emitter layer, free electrons from the TCO have to recombine loss free with holes from the emitter layer. This requires a large dopant density in both layers [17]. However, the ZnO:B implemented in the SHJ solar cells, chosen due to the lowest resistivity of all investigated doping ratios, has a low doping fraction of ~0.025 [5] and will thus have a low dopant density. This might have a severe negative influence on the *FF*, a behaviour that is especially pronounced for low work function TCOs [17].

A way to minimize these possible negative effects of the work function could be a careful adjustment of the interface between the TCO and the emitter layer. By taking advantage of the highly controllable nature of the ALD process, the work function of the TCO could be optimally engineered using e.g. gradual doping [18] or by mixing in a small fraction of a metal other than zinc. For example, ITO-doped ZnO can reach work functions of 4.8 eV and in combination with post deposition treatment even 5.1 eV [19]. Alternatively, indium doped zinc oxide (IZO) can be fabricated with a tuneable bandgap between 4.59 eV and 5.56 eV [20]. Using a similar material would possibly still lower the usage of indium compared to simple ITO films.

For ALD prepared hydrogenated indium oxide (In_2O_3:H), it is expected that hydrogen- and oxygen-containing species effuse from the In_2O_3:H upon annealing. Due to a reaction with the silver contacts, this might lead to an insulating layer between the TCO and silver [21]. To study whether similar effects occur in the case of ALD prepared ZnO:B, which also uses water vapor during the deposition, we pre-annealed sample type IV before depositing the front contacts. To further inhibit oxidation of the metal grid, gold is chosen as contact material. The finished cells are then consecutively annealed while monitoring the *FF* and V_{oc} after each annealing step. Since no improvement in *FF* is seen for these cells compared to cell type I, we rule out that contact oxidation plays a major role as a *FF* limiting factor.

As can be seen in Figure 6, annealing of the cells, even to 240°C, does not have a significant effect on the fill factor. Also the V_{oc}, an indicator for the solar cell´s passivation, stays remarkably stable. This is in sharp contrast to the passivation behavior observed on conventional passivation layer stack containing a-Si:H(p) layers (not using nc-SiO_x:H), showing deterioration already upon annealing at moderate temperatures of 220°C [22] or even 150°C [23].

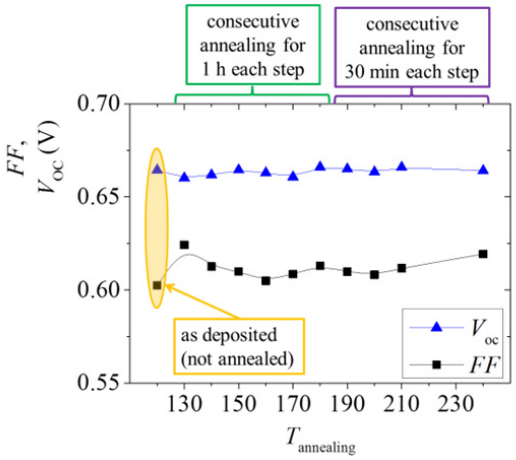

Fig. 6. *FF* and V_{oc} of cell type IV after annealing at different temperatures $T_{annealing}$.

Up to 200°C, the absence of changes in the *J-V* characteristics could be attributed to the prior exposure of the semi cells (including all silicon layers, the backside ITO and Ag contacts) to 200°C during ZnO:B deposition. For higher temperatures up to 240°C, the material characteristics of the nc-SiO_x:H(p) material might play a role in the preserving of the solar cells passivation properties. In an earlier work, we have attributed the tolerance of the passivation properties to high temperatures to the prohibition of hydrogen effusion from the buffer layer by the nc-SiO_x:H(p) layer [24].

4. Conclusion

ZnO:B grown with the novel dopant source TIB has successfully been implemented as indium-free TCO in the front side of SHJ solar cells. Indium free SHJ solar cells have been realized using ZnO:B as front TCO and ZnO:Al as backside TCO. The exceptional high achieved J_{sc} presents a good starting point for further research on ZnO:B as indium free TCO for SHJ solar cells. The use of TIB presents an easily controllable, and presumably much safer alternative in ALD processes to the commonly used highly toxic diborane. Due to a comparably higher series resistance, lower parallel resistance and probably a too low work function of the ZnO:B, a decrease in fill factor compared to cells with standard ITO is observed. A negative effect on the *FF* due to formation of an oxide interlayer between the ZnO:B and the emitter layer has been ruled out. The solar cells show remarkable thermal stabilities up to annealing temperatures of 240°C. Investigation into the influence of the ZnO:B work function and careful engineering of the Si-TCO interface should result in increased efficiency.

Acknowledgements

The authors would like to thank Dr. Yinghuan Kuang and Pim W. Veldhuizen for scientific discussions, Leo A. A. Duval for his help regarding the ZnO:Al, and Ioannis Poulis, Jeroen van Gerwen, Klaas J. Bakker, and Christian A. A. van Helvoirt for technical support. Air Liquide is acknowledged for the donation of the TIB precursor. This research is part of the FLASH program, supported by the Dutch Technology Foundation STW, which is part of the Netherlands Organization for Scientific Research (NWO), and which is partly funded by the Ministry of Economic Affairs.

References

[1] Masuko K, Shigematsu M, Hashiguchi T, Fujishima D, Kai M, Yoshimura N, Yamaguchi T, Ichihashi Y, Mishima T, Matsubara N, Yamanishi T, Takahama T, Taguchi M, Maruyama E, Okamoto S. Achievement of more than 25% conversion efficiency with crystalline silicon heterojunction solar cell. IEEE J Photovolt 2014;4(6):1433-1435.
[2] Air Liquide, Diborane SDS-040-CLP.
[3] Sigma-Aldrich, Triisopropyl borate SDS No. 453/2010.
[4] ChemService, Triisopropylborate SDS NG-17948.
[5] Garcia-Alonso D, Potts SE, Helvoirt CAA, Verheijen MA, Kessels WMM. Atomic layer deposition of B-doped ZnO using Triisopropyl Borate as the Boron precursor and Comparison with Al-doped ZnO. J Mater Chem 2015;3:3095-3107.
[6] Tiwald T. “PSEMI” Oscillator Model. Woollam Co. News 2006;pp.6–7.
[7] Madan A, Rava P, Schropp REI, von Roedern B. A new modular multichamber plasma enhanced chemical vapor deposition system. Appl Surf Sci 1993;70-71(2):716-721.
[8] Kirner S, Mazzarella L, Korte L, Stannowski B, Rech B, Schlatmann R. Silicon heterojunction solar cells with nanocrystaline silicon oxide emitter: insight into charge carrier transport. IEEE J Photovolt 2015;5(6):1601-1605.
[9] Kim S, Yoon H, Kim DY, Kim S-O, Leem J-Y. Optical properties and electrical resistivity of boron-doped ZnO thin films grown by sol-gel dip-coating method. Opt Mater 2013;35(12):2418–2424.
[10] Tahar RBH, Tahar NBH. Boron-doped zinc oxide thin films prepared by sol-gel technique. J Mater Sci 2005;40:5285.
[11] Kumar V, Singh RG, Purohit LP, Mehra RM. Structural, transport and optical properties of boron-doped zinc oxide nanocrystalline. J Mater Sci Technol 2011;27(6):481.
[12] Rößler R, Leendertz C, Korte L, Mingirulli N, Rech B. Impact of the transparent conductive oxide work function on injection-dependent a-Si:H/c-Si band bending and solar cell parameters. J Appl Phys 2013;113:144513.
[13] Varache R, Kleider JP, Gueunier-Farret ME, Korte L. Silicon heterojunction solar cells: Optimization of emitter and contact properties from analytical calculation and numerical simulation. Mat Sci Eng B 2013;178:593–598
[14] Bivour M, Schröer S, Hermle M. Numerical analysis of electrical TCO / a-Si:H(p) contact properties for silicon heterojunction solar cells. Energy Procedia 2013;38:658–669
[15] Klein A, Körber C, Wachau A, Säuberlich F, Gassenbauer Y, Harvey SP, Proffit DE, Mason TO. Transparent Conducting Oxides for Photovoltaics: Manipulation of Fermi Level, Work Function and Energy Band Alignment. Materials 2010;3:4892-4914.
[16] Chen A, Zhu K. Computer simulation of a-Si/c-Si heterojunction solar cell with high conversion efficiency. Solar Energy 2012;86:393-397
[17] Kirner S, Hartig M, Mazzarella L, Korte L, Frijnts T, Scherg-Kurmes H, Ring S, Stannowski B, Rech B, Schlatmann R. Energy Procedia 2015;77:725-732.
[18] Macco B, Deligiannis D, Smit S, van Swaaij RACMM, Zeman M, Kessels WMM. Influence of transparent conductive oxides on passivation of a-Si:H/c-Si heterojunctions as studies by atomic layer deposited Al-doped ZnO. Semicond Sci Technol 2014;29(12200):5pp.
[19] Tsai C-L, Lin Y-J, Wu P-H, Chen S-Y, Liu D-S, Hong J-H, Liu C-J, Shih Y-T, Cheng J-M, Chang H-C. Induced increase in surface work function and surface energy of indium tin oxide-doped ZnO films by (NH4) 2Sx treatment. J Appl Phys 2007;101:113713.
[20] Huang C, Wang M, Deng Z, Cao Y, Liu Q, Huang Z, Liu Y, Guo W, Huang Q. Low content indium-doped zinc oxide films with tunable work function fabricated through magnetron sputtering. Semicond Sci Technol 2010;25:045008 (6pp).
[21] Barraud L, Holman ZC, Badel N, Reiss P, Descoeudres A, Battaglia C, de Wolf S, Ballif C. Hydrogen-doped indium oxide/indium tin oxide bilayers for high-efficiency silicon heterojunction solar cells. Sol Energ Mat Sol Cells 2013;115:151-156.
[22] de Wolf S, Kondo M. Nature of doped a-Si:H/c-Si interface recombination. J Appl Phys 2009;105(103707):1-6.
[23] Schüttauf JWA, van der Werf CHM, Kielen IM, van Sark WGJHM, Rath JK, Schropp REI. Improving the performance of amorphous and crystalline silicon heterojunction solar cells by monitoring surface passivation. J Non-Cryst Solids 2012;385(17):2245-2248.
[24] Gatz HA, Rath JK, Verheijen MA, Kessels WMM, Schropp REI. Silicon heterojunction solar cell passivation in combination with nanocrystalline silicon oxide emitters. submitted to Phys Stat Sol (a).